Benchmarking of Photocatalytic Pigments for Coatings Applications

Ana Carolina Ferreira da Silva Vaz

Instituto Superior Técnico

Abstract—Photocatalytic coatings are a broad field of study where these films are proved to provide the applied surfaces several features such as self-cleaning properties, anti-fouling/anti-bacterial properties, and degradation of pollutants features. Pigments, a component of the coating, may prompt reactions which favour the aforementioned applications when under the action of light - also know as photocatalytic pigments. TiO_2 nanoparticles (NPs) are one of the most used as photocatalytic pigments. However, EU published a statement in 2020 acknowledging its toxicity by inhalation and its potential carcinogenic risks. Regulations applied on this suspected carcinogen material, triggered the need to find healthier and more environmentally-friendly alternatives. A set of alternatives already in use in coatings industry was selected and a benchmarking approach was taken in order to compare and evaluate the selection to the state-of-the-art TiO_2 P25. As TiO_2-based photocatalysts, TiO_2 Rutile, TiO_2 Anatase, TiO_2 P25, ZnO were studied, and as non-TiO_2-based photocatalysts, Fe_2O_3 spherical, Fe_2O_3 lamellar, FeOOH, and Cu_2O were characterized and tested. The characterization techniques involved X-Ray Diffraction (XRD) and UV-Vis Diffuse Reflectance Spectroscopy (DRS). The first, revealed the structure, the relative quantity of each present phase, and the cristallite size.All the pigments were tested in the photodegradation of methylene blue in aqueous solution followed by UV-Vis spectroscopy using UV-C and UV-Vis light. UV-Vis-DRS along with the Kubelka-Munk equation gave out the band gap value. Of all the non-TiO_2-based alternatives studied, ZnO was elected the alternative to TiO_2-based photocatalysts. It showed the best performance under both types of light when compared with TiO_2-based samples.

Keywords—Coatings; photocatalysis; semiconductor; methylene blue photodegradation; non-TiO_2 based photocatalysts; TiO_2 nanoparticles; toxicity; X-ray diffraction; UV-Vis Diffuse reflectance spectroscopy; UV light source.

1 Introduction

A Coating is a layer of material which is applied to a surface, commonly known as paint or varnish, and may have several purposes, such as decorative or protective purposes. Pigments, a component of the coating, may unveil photocatalytic properties. Photocatalysis is a mechanism where photocatalytic materials, when hit by light, may promote reduction and oxidation reactions. Having light as the driving force, the final applications are the most diverse - from self-cleaning surfaces to the degradation of air pollutants, and the inactivation of viruses and bacteria [1], [2].

Even though photocatalytic coatings contribute to the sustainable development of communities, which is in accordance with UN's Sustainable Development Goals [3], there are some drawbacks that need to be addressed. Recently, the widely used TiO_2 NPs, have been defined as suspicious carcinogen to humans by inhalation - published at the latest EU Regulation on classification, labelling and packaging (CLP) of substances and mixtures [4]. As these harmful effects are being brought to light, leading political entities are putting pressure on the scientific community to come up with new ideas to solve these problems.

The main objective of this work is to select and compare a set of photocatalytic pigments already in use in the industry. A benchmarking approach put TiO_2-based photocatalysts against non-TiO_2-based alternatives. The TiO_2 photocatalytic pigment was selected because it is an acknowledged state-of-the-art pigment. As a result of the literature review, the fol-

• *Ana Carolina Ferreira da Silva Vaz, no. 81104, E-mail: acarolinavaz@tecnico.ulisboa.pt,*

Submitted November, 2021

lowing non-TiO_2-based materials were studied: Fe_2O_3 (spherical and lamellar), FeOOH, ZnO, and Cu_2O. Their photocalatytic activity have not been extensively described in literature, but some work have pointed this semiconductors out as potentially active within UV-Vis light. TiO_2-based photocatalysts materials were chosen to compare and evaluate alternative's performance. Those are TiO_2 rutilo, TiO_2 anatase, and TiO_2 P25. Before the performance evaluation, characterization techniques were executed, such as the X-ray diffraction (XRD) and Diffuse reflectance spectroscopy (DRS). After that, some protocols found in the literature, to evaluate the performance of each pigments, were adopted. Under two types of light sources photocatalytic tests were carried out: UV-C and a "more realistic" UV-Vis light bulbs. A slurry composed of one of the pigments and a dye, methylene blue (MB) in this case, was prepared and put under these light sources. The degradation of the dye was confirmed and measured by means of a spectrophotometer, being the semiconductor's performance subsequently evaluated.

2 EXPERIMENTAL

2.1 Materials

To evaluate each sample's performance, its ability to degradate a dye under the influence of light was studied using Methylene Blue (MB) (Sigma-Aldrich, 97% purity, dry basis). Distilled water (DW) served as dispersion medium.

All the samples in study are summarized in Table 1. The two light sources characteristics are summarized in Table 2.

2.2 Characterization

The characterization of the samples was done resorting to two techniques in order to obtain comprehensive information on the physicochemical, structural, and morphological properties of the samples.

Powder X-ray diffraction (XRD) patterns were acquired in a D8 Advance diffractometer from Bruker equipped with a Cu lamp (CuKα = 1.5406 Å), a 1D LynxEye detector and a Ni filter. Experiments were performed from 5 to 80 ° (2 θ) with a step size of 0.05 ° and a step time of 1s. Results were analyzed with TOPAS software (version 5.2) from Bruker.

The UV-Vis spectra of each pigment were obtained using the Cary 5000 spectrophotometer from Varian equipped with a Praying mantis accessory for DRS measurements. The information was recorded sweeping wavelengths from 200 up to 2500 nm. The scans were obtained with a spectral bandwidth of 4 nm, a scan rate of 600 nm/min, and a data interval of 1 nm. From this technique the band gap value, which helps to evaluate on the sample performance, may be obtained. Resorting to the Kubelka-Munk theory - which covers the behaviour of light flux through homogeneous isotropic media - it is possible to relate the diffuse reflected light to the absorption coefficient, K [5]. The fundamental equation goes as follows.

$$F(R_{inf}) = \frac{K}{S} = \frac{(1 - R_{inf})^2}{2R_{inf}} \quad (1)$$

Being S the backscattering coefficient and R_{inf} the remission fraction of an infinitely thick layer. Both S and K are defined by the corresponding thickness of the layer. It is assumed that S changes negligibly within the wavelength region of electronic absorption being the Kubelka-Munk function solely dependent on K. This assumption facilitates the calculations in a way that the absorption, α, can be related to K using the Tauc relation [5]–[7].

$$F(R_{inf}) \cdot hv)^{\frac{1}{n}} \sim (\alpha \cdot hv)^{\frac{1}{n}} \quad (2)$$

h being the Planck's constant, v the speed of light, α the absorption coefficient, n the type of electronic transition, and Eg the optical band gap energy.

Being h the Planck's constant, v the speed of light, α the absorption coefficient, n the type of electronic transition, and Eg the optical band gap energy.

From the benchmarking point of view, the comparison between potential candidates to find alternatives to TiO_2-based photocatalysts demands a systematic protocol for achieving reproducible and meaningful results. The adopted method to find the Eg value consists

Table 1: List of the samples used. Purity and supplier.

Sample	Supplier	Commercial Reference	Composition (%)
TiO_2 P25	Sigam-Aldrich	Aeroxide	99.5
TiO_2 rutile	Chemours Company	-	97
TiO_2 anatase	Merk	-	99
ZnO	EverZinc	-	99.9
Fe_2O_3 lamellar	Promindsa	Micronox R01	76-95
Fe_2O_3 spherical	Promindsa	Micronox R110	76-95
FeOOH	Lanxess	Bayferrox 943	99.4
Cu_2O	Nordox	-	99

Table 2: Model and characteristics of the source of light.

Name	Philips	Exo-Terra
Model	TUV 4P SE UNP/32	Reptil Glo 10.0 T8
Power (W)	16*6	14*6
Light Source	UV-C (250 nm)	UV + Visible

in making linear regressions. Although quite sensible to interpretation, this empirical way of obtaining the *Eg* value is acknowledged and very much used by the scientific community. Depending on the spectrum profile, one or two tangent lines are drawn assuming in this last case the intersection to be the *Eg* value [8]. Those lines were drawn tangent to the far left curve, on the first method, or tangent to the two far left curves of the plot, on the second method. Figures 1 and 2 illustrate these methods.

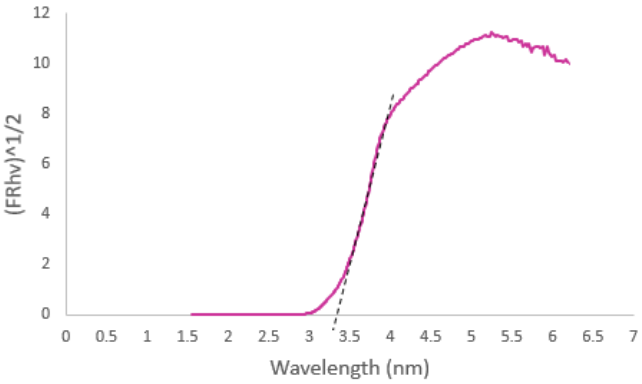

Figure 1: Example of a Tauc Plot obtained with the first method (TiO_2 P25).

2.3 Photocatalysis

In a 1 L flask a solution of MB was prepared and agitated magnetically for 1 h using aluminium foil as a light shield. In a 250 mL Erlenmeyer, each pigment and 250 mL of MB solution were added and the flask was covered

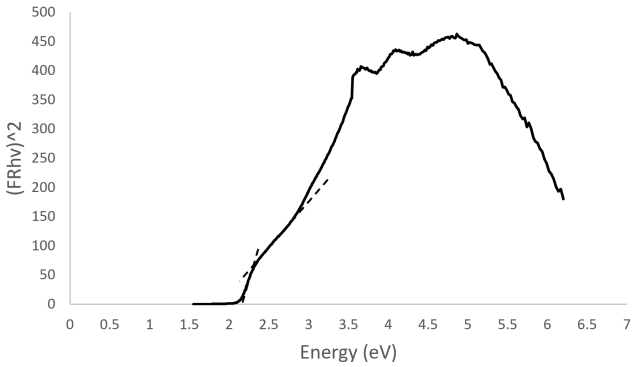

Figure 2: Example of a Tauc Plot obtained with the second method (Fe_2O_3 lamellar).

in aluminium foil to prevent an uncontrolled photocatalytic reaction due to unwanted exposure to ambient light. The mixture was then sonicated for 15 min and magnetically stirred at 2000 rpm for 1 h in the dark to assure the adsorption-desorption equilibrium. Past that hour, a sample was withdrawn, and the absorbance was measured to evaluate the MB absorbance by the catalyst. After that, the light was turned on and a sample was withdrawn every 20 min. The absorbance was measured using a spectrophotometer and the temperature was measured. The experiment was carried out until the MB degradation reached around 98% or after 2 h have passed.

Photolysis is the decomposition or separation of molecules by the action of light. In order to check if the studied dye was active when irradiated, a solution of MB was prepared and left under its action for 3h. After building the calibration curve and going through some literature, two concentrations of MB were chosen - 10 mg/L and 20 mg/L and the protocol settled. A 250 mL Erlenmeyer was firstly sonicated for 5 min and then magnetically stirred in the dark

for 1 h to attain homogeneity. Right before the UV-C light was turned on, a sample was withdrawn and its absorbance measured on a spectrophotometer. Right after, the light was turned and a sample was withdrawn every 20 min. Every experiment stopped after three hours.

To withdraw a sample, a syringe and a filter were used. The aim of the filter is preventing the dispersed powder to interfere with the MB solution absorbance measurement. A filter protocol had to be defined to optimize its use. This way, the slurry would easily reach the equilibrium again every time a sample was withdrawn.

3 Results and Discussion

3.1 Structure and Morphology

Samples can be splitted into two groups: the pure ones (having mainly one phase), and the mixed-phase ones (having two or more different phases). Resorting to the profile fitting based software TOPAS, and to COD and PDF databases, the quantitative phase analysis, microstructure analysis and crystal structure analysis information was obtained. To mention that the method behind the fitting based software TOPAS, and discribed elsewhere, is the Rietveld method [9].

The information obtained is summarized in Table 3.

ZnO, Fe_2O_3 spherical, FeOOH, and Cu_2O samples present only one phase. On the other hand, TiO_2 P25, TiO_2 rutile, TiO_2 anatase, and Fe_2O_3 lamellar are mix-phased. The Fe_2O_3 lamellar have four different phases, namely hematite, dolomite, quartz, and mica. The commercialized TiO_2 P25 (Sigma-Aldrich) diffraction peaks corresponded to reference line patterns - anatase (87 wt.%) and rutile (13 wt.%) - which confirmed the crystalline structure of TiO_2 P25. These findings are in agreement with the information provided by the supplier and with the structural analysis reported in the literature [10]. Also, TiO_2 rutile has a second phase, anatase, although representing only around 0,7% of the global weight. The same happens for TiO_2 anatase, where the rutile phase only accounts for 1.8% of the total weigth.

Figure 3 and 4 are examples of XRD patterns - one and more phases sample, respectively.

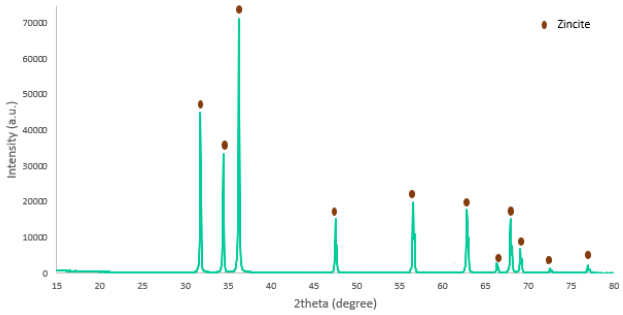

Figure 3: Example of a one phase sample diffractogram (ZnO) - zincite COD 9004180.

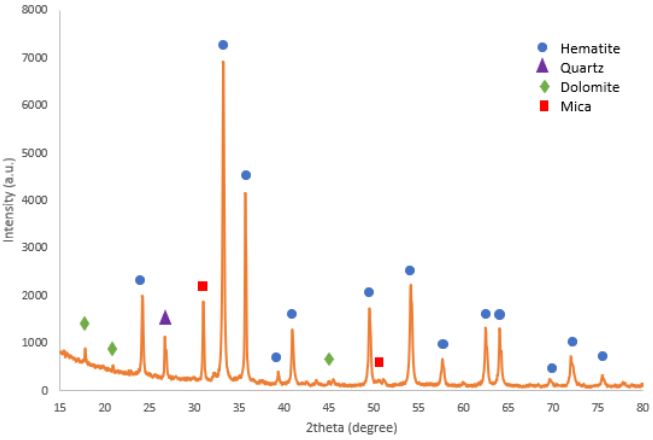

Figure 4: Example of a mixed-phase sample diffractogram (Fe_2O_3 lamellar) - hematite, dolomite, quartz, and mica - COD 9015964, COD 2105963, PDF 46-1045, and PDF 07-0042, respectively.

The TiO_2-based photocatalytic main phases, anatase and rutile, are acknowledged photocatalyic active structures [11]. On the other hand, non-TiO_2 - photocatalyst main phases - hematite, goethite, cuprite, zincite - are still in study [12]–[15]. This belief supported by several articles encouraged the determination of their potential as photocatalysts. Quartz and mica are used as sand to improve the appearance and durability of architectural and industrial paint and coatings or to promotes paint adhesion in aqueous and oleoresinous formulations [16]. Dolomine may work as a photocatalyst, but that was not verified, most

Table 3: XRD analysis experimental data. Mean particle size available on the supplier's data sheets. *NI* means no information.

Sample	Phase	Weigth %	Crystallite Size (nm)	Mean Particle Size (nm)
TiO_2 P25	Anatase/Rutile	87/13	21/33	21
TiO_2 rutile	Anatase/Rutile	1/99	126	290
TiO_2 anatase	Anatase/Rutile	98/2	105	NI
ZnO	Zincite	100	125	NI
Fe_2O_3 lamellar	Hematite/Dolomite/Quartz/Mica	91/2/2/5	53	NI
Fe_2O_3 spherical	Hematite	100	50	NI
FeOOH	Goethite	100	54	50 - 300
Cu_2O	Cuprite	100	33	NI

likely due to its wide band gap value, 5,02 eV [17].

Regarding crystallite size, TiO_2 rutile, TiO_2 anatase, and ZnO have a crystallite size superior to 100 nm, may being considered a microstructure. Among white pigments, TiO_2 P25 is the only with a nanostructure (21/33 nm). Fe-based have around the same crystallite size (50 nm), while Cu_2O has a smaller size, 33 nm. Worth mentioning that the state-of-the-art TiO_2 P25 also matched the anatase:rutile ratio [11].

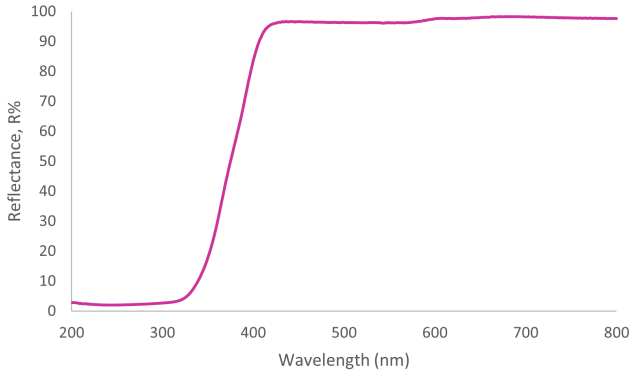

Figure 5: TiO_2 P25 reflectance plot.

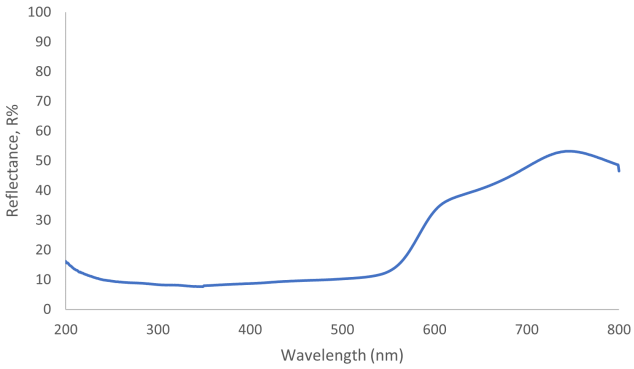

Figure 6: Fe_2O_3 lamellar reflectance plot.

3.2 Optical Properties

Absorbance TiO_2-based photocatalysts and ZnO present the same absorption threshold. All four absorb light under the 400 nm (UV band). All the radiation higher than 400 nm is reflected. Regarding Fe_2O_3 spherical and lamellar they both absorb radiation below 600 nm. FeOOH absorbs for lower wavelengths than 500 nm. Cu_2O absorbs for lower values than 600 nm. All the Fe-based samples and Cu_2O absorb light in part of the UV-Vis region. This behavior in the UV-Vis region, proved them to be potential photocatalysts. Figure 5 and 6 are two examples of the reflance plots obtained by the spectrophotometer.

Band Gap The reflectance plots obtained by the UV-Vis DRS were converted to Kubelka-Munk functions, Equation 1. Both direct and indirect electronic transitions were plotted and the band gap obtained. On tables 4 and 5 the band gap value obtained, as well as the band gap literature value and the type of electronic transition may be consulted - [18]–[23].

White samples band gap values are in accordance with the literature - 4. In the case of colour samples, the difference is noticeable

Table 4: Experimental electronic characteristics of the samples and the value found on literature. One tangent line approach.

Sample	Band Gap Direct	Band Gap Indirect	Band Gap Literature
TiO_2 P25	3.7	3.3	3.20
TiO_2 rutile	3.2	3.2	3.00
TiO_2 anatase	3.4	3.2	3.20
ZnO	3.3	3.2	3.25

Table 5: Experimental electronic characteristics of the samples and the values found on literature. Obtained band gap using the tangent lines intersection method.

Sample	Band Gap Direct	Band Gap Indirect	Band Gap Literature
Fe_2O_3 lamellar	2.3	2.4	1.97
Fe_2O_3 spherical	2.3	2.4	1.97
FeOOH	2.7	2.7	2.15
Cu_2O	2.0	2.0	2.35

- Table 5. The possibility of more transitions favoured by the interaction with the visible radiation can explain the so complex profile of the colour pigments. That behaviour contributes to a less consensual approach of this practical method once it depends entirely on the operator's judgement. This can make the confrontation of experimental data with the literature challenging, which urges the need to adopt a systematic and straightforward approach so results may be compared and conclusions are drawn more easily.

3.3 Photocatalytic Performance

The change in the absorption spectra of the dye was monitored at regular intervals of time. The degradation behavior of all the samples for methylene blue can be seen in Figure 7 and 8.

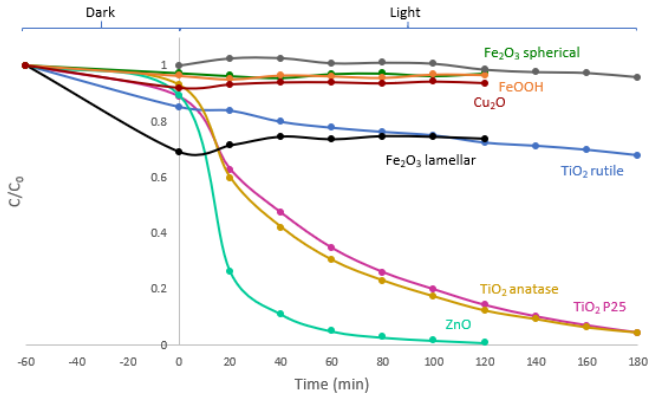

Figure 7: MB (10 mg/L) degradation by the catalyst (400 mg/L) under UV-C light.

In the Dark, it is believed not to occur MB degradation. The decrease of C/C_0 in the dark, spotted in Figures 7 and 8, may be explained by the adsorption of the dye by the photocatalyst phenomenon, once no degradation is excepted. The Fe_2O_3 lamellar is the sample that adsorbs the most. That may be due to its lamellar structure, which may trap more MB

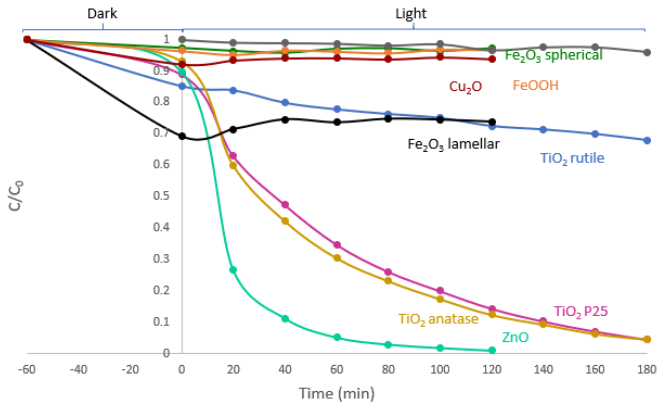

Figure 8: MB (10 mg/L) degradation by the catalyst (400 mg/L) under UV-Vis light.

molecules. To check this assumption, further calculations should be performed. Also, further experiments could be performed to sustain this premise, such as building the profile of MB adsorption by the Fe_2O_3 lamellar and also studying the textural properties of the powder (i.e N_2-adsorption).

UV-C light

Under UV-C illumination, different degradation behaviours have been registered. TiO_2 P25, TiO_2 rutile, TiO_2 anatase, and ZnO are the pigments with the best MB degradation performance. ZnO showed a MB degradation of around 100% after 2 h while TiO_2 P25, and TiO_2 anatase degraded more than 90% after 3 h. TiO_2 rutile went no further than 20% after 3 h. Fe-based and Cu_2O samples revealed the lowest activity under light exposure holding around 0% MB degradation after 3 h.

UV-Vis light

Under UV-Vis illumination, the degradation behaviour registered revealed an identical behaviour to the UV-C light. TiO_2 P25, TiO_2 rutile, TiO_2 anatase, and ZnO were again the pigments with the best MB degradation performance. ZnO showed a MB degradation of around 100% after 2 h while TiO_2 P25, and TiO_2 anatase degraded more than 90% after 3 h. TiO_2 rutile went no further than 20% after 3 h. Fe-based and Cu_2O samples revealed the lowest activity under light exposure holding around 0% MB degradation after 3 h.

The best photo-degradation performance belongs to TiO_2 P25, TiO_2 rutile, TiO_2 anatase, and ZnO - white pigments. The Fe-based and

Cu_2O are the powders which revealed lower to none activity under light exposure - colored pigments.

3.4 Kinetic Study

Heterogeneous photocatalysis follows a Langmuir-Hinshelwood model, which may be written as 4.

$$\frac{1}{r} = \frac{1}{k_r k_a C} \tag{3}$$

r is the reaction rate for the oxidation of reactant, kr is the specific reaction rate constant for the oxidation of the reactant (mg/Lmin), ka is the equilibrium constant of the reactant (L/mg) and C is the dye concentration. When C_0 is small (milimolar) the equation can be simplified to as apparent first-order equation [24].

$$C = C_0 exp(-k_{app} t) \tag{4}$$

To analyse the data, a normalized form of Langmuir-Hinshelwood, should be plotted in order to describe the solid-liquid reaction 5 [25].

$$ln\frac{C}{C_0} = -kt \tag{5}$$

Figures 9 and 10 represent the kinetic model of the MB degradation under UV-C and UV-Vis following that model.

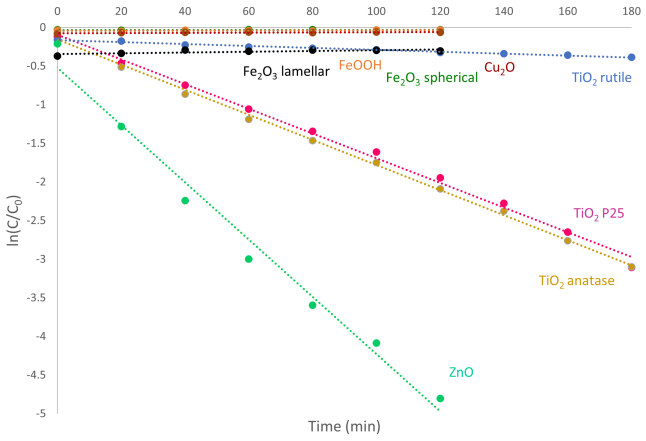

Figure 9: Kinetic model: MB (10 mg/L) degradation by the catalysts (400 mg/L) under UV-Vis.

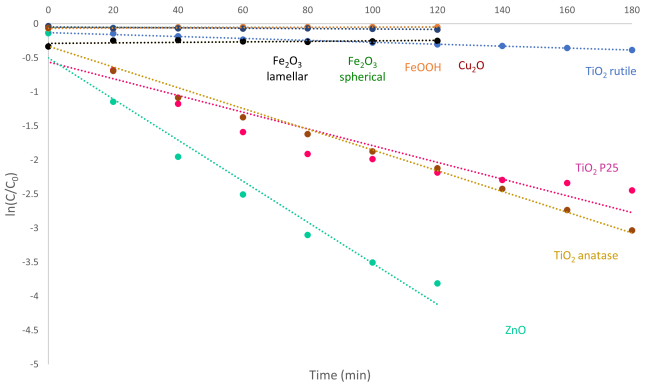

Figure 10: Kinetic model: MB (10 mg/L) degradation by the catalysts (400 mg/L) under UV-C.

The reaction rate constant for both light sources and runs, are in Table 6. The Fe-based samples, as well as Cu_2O, are not represented here because the regression did not provide realistic rate constants, ranging from (0.002 to 0.05)10^{-2} min^{-1} in absolute value.

Table 6: Constant for each light source (UV-C and UV-Vis) and for both runs.

Powder	**kx10^{-2} (min^{-1}) UV-C**	**kx10^{-2} (min^{-1}) UV-Vis**
TiO_2 P25	1.2 / 2.3	1.3 / 1.6
TiO_2 rutile	0.14 / 0.16	0.13 / 0.17
TiO_2 anatase	1.5 / 1.7	1.4 / 1.6
ZnO	3.0 / 3.5	3.6 / 3.7

All the pigments confirmed the pseudo first-order kinetics fitting ($0.8758 < R^2 < 0.9886$).

UV-C light

In Figure 10, TiO_2 P25, TiO_2 anatase, and ZnO are the samples which showed the best performance - TiO_2 P25 (1.20x10^{-2} min^{-1}) < TiO_2 anatase (1.50x10^{-2} min^{-1}) < ZnO (3.00x10^{-2} min^{-1}). TiO_2 rutile, among the best performances, is the one with the lowest reaction rate constant - 0.14x10^{-2} min^{-1}. As said previously, Fe-based and Cu_2O did not provide realistic constants.

UV-Vis light

In Figure 9, TiO_2 P25, TiO_2 anatase, and ZnO are the samples which showed the best performance - TiO_2 P25 (1.30x10^{-2} min^{-1}) < TiO_2 anatase (1.40x10^{-2} min^{-1}) < ZnO (3.50x10^{-2} min^{-1}). TiO_2 rutile, among the best performances detained by the white powders, is the one with the lowest reaction rate constant - 0.13x10^{-2} min^{-1}. As said previously, Fe-based and Cu_2O did not provide realistic constants.

The band gap value may give an idea of how good a sample is under a certain type of light source. Narrower band gaps (colour samples) need less energetic light to form a pair electron/hole. On the contrary, wider band gaps (white pigments) need more energy for a pair electron/hole to occur. The band gap width was obtained to comply with the absorbance region of the samples covered before. Meaning, wider band gap semiconductors have an electron/hole pair with more potential energy than the pairs formed in narrower band gaps.

Once UV light accounts for only around 8% of the spectrum of light, that makes wide band gaps less active under sunlight and indoor environments where common light has almost no UV component. Narrower band gap semiconductors will need less energetic light to form an electron/hole pair (UV-Vis). In short, wider band gap semiconductors will have their applications shortened under sunlight and indoor light.

In short, colour pigments showed a low activity under both types of lights, while white pigments showed better performance under UV-C and UV-Vis - as k values suggest (Table 6). However, there is another aspect that should be taken into consideration when evaluating pigments performance - the VB/CB position, Figure 11.

Photocatalytic degradation is a surface reaction, therefore, high surface areas generally promote higher degradation since the pollutants adsorb faster onto the catalyst surface. The smaller particle size, the higher the surface are. The white pigments - ZnO, anatase, and rutile - have particle sizes superior to 100 nm. Only P25 has a particle size of 21/33 nm. All the colored ones have a particle size of 33 - 54 nm. Regarding what was explained previously, the lower particle size should present a better photodegradation performance. However, the light used was not enough to promote the reaction.

The band gap position may enable reduction and/or oxidation reactions depending on the positions of the VB/CB [27]. The VB hole formed when the migration of the electron to the conduction band is a strong oxidizing agent and it is capable of oxidizing electron donor molecules adsorbed on the surface. The CB electron is a powerful reducing agent and may reduce acceptor molecules.

Wider band gap samples, namely TiO_2 P25, TiO_2 anatase and ZnO, have their valence and conduction bands well aligned to trigger oxidation and reduction reactions. The proper alignment, along with the wide band gap, grant these samples the best photocatalytic performance. The narrower band gap samples present a lower to none activity because of the band alignment which does not allow reduction reactions to occur.

4 Conclusions and Future Work

The main objective of this work was to select and compare a set of photocatalytic pigments already in use in the industry. A benchmarking approach put TiO_2-based photocatalysts against non-TiO_2-based alternatives. The TiO_2 photocatalytic pigment was selected because it is an acknowledged state-of-the-art pigment.

All the samples in the study were characterized using techniques that gave out information about their physicochemical, structural, and optical properties, namely XRD and UV-DRS techniques. Pigments have shown the presence of one or more phases. In the case of TiO_2 rutile, TiO_2 anatase, ZnO, Cu_2O, Fe_2O_3 spherical, and FeOOH they are all pure - having the first two minute quantities of other phases (TiO_2 rutile with 1 wt.% anatase and TiO_2 anatase with 2 wt.%). On the other hand, Fe_2O_3 lamellar, and TiO_2 P25 revealed the presence of two or more phases. The TiO_2-based photocatalysts main phases, anatase and rutile, are acknowledged photocatalytic active structures. Oppositely, non-TiO_2-photocatalyst main phases - hematite, goethite, cuprite, zincite - are still in study. Fe_2O_3 lamellar has four different phases - hematite, dolomite, quartz, and mica.

The photo-degradation protocol revealed pigments performances. ZnO is the only non-TiO_2-based pigment which showed a better performance than TiO_2 P25 under UV-C and UV-Vis lights. Fe_2O_3 lamellar, Fe_2O_3 spherical, FeOOH, and Cu_2O did not degrade methylene blue, while TiO_2 rutile, TiO_2 anatase, and TiO_2 P25 did degrade the dye at some extent. Not

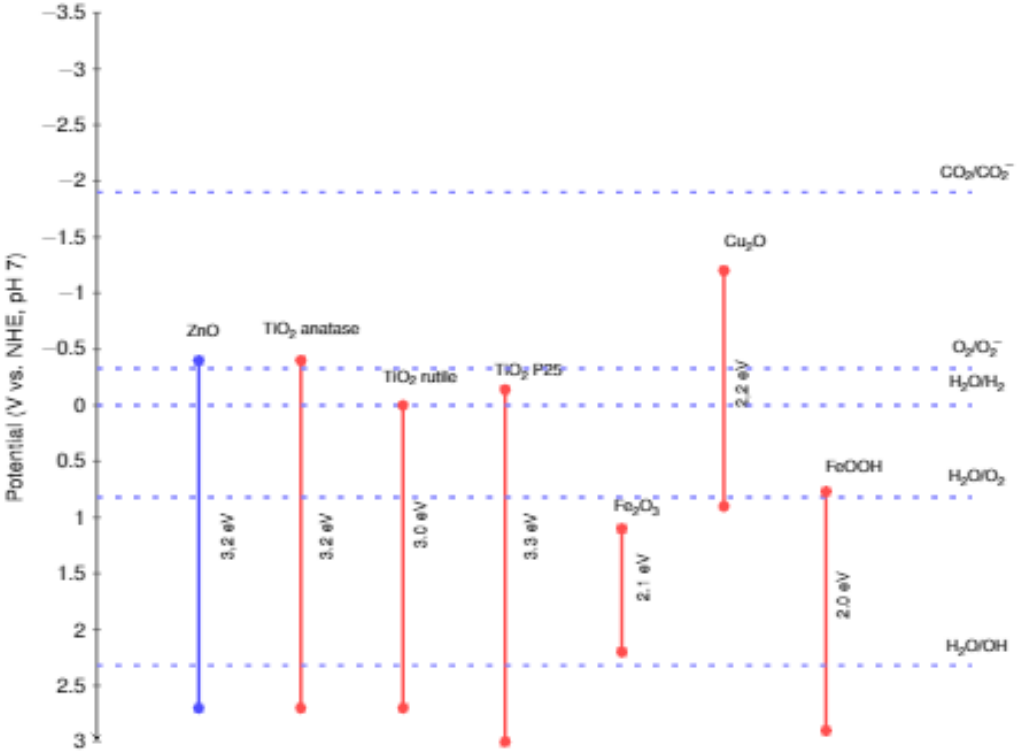

Figure 11: Valence and conduction band samples' position [26].

only does the band gap value dictate the efficacy of a photocatalytic pigment, but few other aspects such as the position of the valance and conduction band. ZnO band's position enables oxidation and reduction reactions to occur.

Even though ZnO proved to be a good alternative to TiO_2-based photocatalysts, further characterization must be done as well as photodegradation experiments. Regarding characterization, SEM should be carried out to corroborate XRD results and confirm the structure. N2-physisorption and DLS techniques should be performed again. The first will give out information about the textural properties of the sample, while the latter will determine the size distribution profile of the particles, corroborating, or not, the XRD results. Adopting other types of light sources, with less UV component and more Vis component, would be interesting to evaluate the performance of each sample under this less energetic light source. And lastly, elected the ZnO, the formulation of a photocatalytic coating containing this pigment and the evaluation of its activity, including comparison with reference coatings containing TiO_2 NPs, should be performed.

Acknowledgments

Thank you to my supervisors, Dr. Auguste Fernandes (IST), Prof. Dr. Amado Velázquez-Palenzuela (DTU) for the guidance. The pandemic decreased the available time frame and forced to alter the course of this project, so the fact that this manuscript has been produced at all is due to all the support I received.

References

[1] E. Luévano-Hipólito, L. M. Torres-Martínez, and L. V. Cantú-Castro, "Self-cleaning coatings based on fly ash and bismuth-photocatalysts: Bi2O3, Bi2O2CO3, BiOI, BiVO4, BiPO4," *Construction and Building Materials*, vol. 220, pp. 206–213, 2019.

[2] S. Douven, J. G. Mahy, C. Wolfs, C. Reyserhove, D. Poelman, F. Devred, E. M. Gaigneaux, and D. Lambert, "Efficient N, Fe Co-Doped TiO2 Active under Cost-Effective Visible LED Light: From Powders to Films," no. x.

[3] "Sustainable Development Goals - UNITED NATIONS." [Online]. Available: https://www.undp.org/sustainable-development-goals?utm{_}source=EN{\&}utm{_}medium=GSR{\&}utm{_}content=US{_}UNDP{_}PaidSearch{_}Brand{_}English{\&}utm{_}campaign=CENTRAL{\&}c{_}src=CENTRAL{\&}c{_}src2=

GSR{\&}gclid=EAIaIQobChMI4cGov93d8wIVzt{_}tCh2DLAEXEAAYBCAAEgLOPPD{_}BwE

[4] E. Union Commission Delegated Regulation (EU), "Mixtures containing titanium dioxide," vol. 10, no. December 2016, pp. 1–21, 2020.

[5] S. Bock, C. Kijatkin, D. Berben, and M. Imlau, "applied sciences Absorption and Remission Characterization of Pure , Dielectric (Nano-) Powders Using Diffuse Reflectance Spectroscopy : An End-To-End Instruction," 2019.

[6] R. Alcaraz de la Osa, I. Iparragirre, D. Ortiz, and J. M. Saiz, "The extended Kubelka–Munk theory and its application to spectroscopy," *ChemTexts*, vol. 6, no. 1, 2020. [Online]. Available: https://doi.org/10.1007/s40828-019-0097-0

[7] P. Makuła, M. Pacia, and W. Macyk, "How to correctly determine the band gap energy of modified semiconductor photocatalysts based on uv-vis spectra," *Journal of Physical Chemistry Letters*, vol. 9, pp. 6814–6817, 12 2018. [Online]. Available: https://pubs.acs.org/doi/full/10.1021/acs.jpclett.8b02892

[8] P. Makuła, M. Pacia, and W. Macyk, "How To Correctly Determine the Band Gap Energy of Modified Semiconductor Photocatalysts Based on UV-Vis Spectra," *Journal of Physical Chemistry Letters*, vol. 9, no. 23, pp. 6814–6817, 2018.

[9] J. P. de Villiers and P. R. Buseck, "Mineralogy and instrumentation," *Encyclopedia of Physical Science and Technology*, pp. 1–27, 1 2003.

[10] E. K. Tetteh, S. Rathilal, and D. B. Naidoo, "Photocatalytic degradation of oily waste and phenol from a local South Africa oil refinery wastewater using response methodology," *Scientific Reports*, vol. 10, no. 1, 2020.

[11] X. Jiang, M. Manawan, T. Feng, R. Qian, T. Zhao, G. Zhou, F. Kong, Q. Wang, S. Dai, and J. H. Pan, "Anatase and rutile in evonik aeroxide P25: Heterojunctioned or individual nanoparticles?" *Catalysis Today*, vol. 300, no. May 2017, pp. 12–17, 2018. [Online]. Available: http://dx.doi.org/10.1016/j.cattod.2017.06.010

[12] K. Qi, B. Cheng, J. Yu, and W. Ho, "Review on the improvement of the photocatalytic and antibacterial activities of ZnO," *Journal of Alloys and Compounds*, vol. 727, pp. 792–820, 2017. [Online]. Available: https://doi.org/10.1016/j.jallcom.2017.08.142

[13] A. A. Jelle, M. Hmadeh, P. G. O'Brien, D. D. Perovic, and G. A. Ozin, "Photocatalytic properties of all four polymorphs of nanostructured iron oxyhydroxides," *ChemNanoMat*, vol. 2, pp. 1047–1054, 11 2016. [Online]. Available: https://onlinelibrary.wiley.com/doi/full/10.1002/cnma.201600251https://onlinelibrary.wiley.com/doi/abs/10.1002/cnma.201600251https://onlinelibrary.wiley.com/doi/10.1002/cnma.201600251

[14] R. A. N. Khasanah, H.-C. Lin, H.-Y. Ho, Y.-P. Peng, T.-S. Lim, H.-L. Hsiao, C.-R. Wang, M.-C. Chuang, and F. S.-S. Chien, "Studies on the substrate-dependent photocatalytic properties of cu2o heterojunctions," *RSC Advances*, vol. 11, pp. 4935–4941, 1 2021. [Online]. Available: https://pubs.rsc.org/en/content/articlehtml/2021/ra/d0ra10681jhttps://pubs.rsc.org/en/content/articlelanding/2021/ra/d0ra10681j

[15] R. Ilmetov, "Photocatalytic activity of hematite nanoparticles prepared by sol-gel method," *Materials Today: Proceedings*, vol. 6, pp. 11–14, 1 2019.

[16] Y. Lee, S. Kim, H. Fei, J. K. Kang, and S. M. Cohen, "Photocatalytic CO2 reduction using visible light by metal-monocatecholato species in a metal-organic framework," *Chemical Communications*, vol. 51, no. 92, pp. 16 549–16 552, 2015.

[17] J. K. Ratan, A. Saini, and P. Verma, "Microsized-titanium dioxide based self-cleaning cement: incorporation of calcined dolomite for enhancement of photocatalytic activity," *MRE*, vol. 5, p. 115509, 11 2018. [Online]. Available: https://ui.adsabs.harvard.edu/abs/2018MRE....5k5509R/abstract

[18] A. Abdolhoseinzadeh and S. Sheibani, "Enhanced photocatalytic performance of Cu2O nano-photocatalyst powder modified by ball milling and ZnO," *Advanced Powder Technology*, vol. 31, no. 1, pp. 40–50, 2020. [Online]. Available: https://doi.org/10.1016/j.apt.2019.09.035

[19] T. Yang, S.-j. Park, T. G. Kim, D. S. Shin, K.-d. Suh, and J. Park, "Ultraviolet photodetector using pn junction formed by transferrable hollow n-TiO_2 nano-spheres monolayer," *Optics Express*, vol. 25, no. 25, p. 30843, 2017.

[20] U. Nwankwo, R. Bucher, A. B. Ekwealor, S. Khamlich, M. Maaza, and F. I. Ezema, "Synthesis and characterizations of rutile-TiO2 nanoparticles derived from chitin for potential photocatalytic applications," *Vacuum*, vol. 161, no. October 2018, pp. 49–54, 2019. [Online]. Available: https://doi.org/10.1016/j.vacuum.2018.12.011

[21] M. C. Borrás, R. Sluyter, P. J. Barker, K. Konstantinov, and S. Bakand, "Y2o3 decorated tio2 nanoparticles: Enhanced uv attenuation and suppressed photocatalytic activity with promise for cosmetic and sunscreen applications," *Journal of Photochemistry and Photobiology B: Biology*, vol. 207, p. 111883, 6 2020.

[22] G. Liu, S. Liao, D. Zhu, L. Liu, D. Cheng, and H. Zhou, "Photodegradation of aniline by goethite doped with boron under ultraviolet and visible light irradiation," *Materials Research Bulletin*, vol. 46, no. 8, pp. 1290–1295, 2011. [Online]. Available: http://dx.doi.org/10.1016/j.materresbull.2011.03.033

[23] P. Kushwaha and P. Chauhan, "Synthesis of spherical and Rod-Like EDTA assisted α-Fe2O3 nanoparticles via Co-precipitation method," *Materials Today: Proceedings*, no. xxxx, 2021. [Online]. Available: https://doi.org/10.1016/j.matpr.2021.02.450

[24] M. A. Rauf and S. S. Ashraf, "Fundamental principles and application of heterogeneous photocatalytic degradation of dyes in solution," *Chemical Engineering Journal*, vol. 151, no. 1-3, pp. 10–18, 2009.

[25] M. A. Rauf, S. B. Bukallah, A. Hamadi, A. Sulaiman, and F. Hammadi, "The effect of operational parameters on the photoinduced decoloration of dyes using a hybrid catalyst V2O5/TiO2," *Chemical Engineering Journal*, vol. 129, no. 1-3, pp. 167–172, 2007.

[26] D. Durgalakshmi, R. Ajay Rakkesh, S. Rajendran, and M. Naushad, "Principles and Mechanisms of Green Photocatalysis," vol. 15110019, no. September 2019, pp. 1–24, 2020.

[27] F. Hamidi and F. Aslani, "Tio2-based photocatalytic cementitious composites: Materials, properties, influential parameters, and assessment techniques," *Nanomaterials*, vol. 9, no. 10, 2019.